Chapter 17
Computational Fluid Dynamics for Evaluating Hemodynamics

David Saloner

Overview

Blood flow in vessels plays an important role in the physiological response of the vasculature in health and disease and in preserving the function of the end organs. While many of the descriptors that are important in evaluating the health of a vascular territory are well established, many others remain the domain of active investigation. The ability to establish the relationship between adverse hemodynamics and patient outcome has dramatically improved with the advent of robust high-resolution, noninvasive imaging measures of the local disease in the vessel wall, the prevailing flow conditions, and the status of the end organ. However, establishing causal connections between hemodynamic descriptors and physiological impact requires detailed knowledge of the spatial and temporal distribution of those descriptors. Computational Fluid Dynamics (CFD) methods are well suited to this task. The ever-increasing power of computational platform resources permits simulations of appropriately complex anatomic models in manageable compute times. In this chapter, the assumptions that underlie the CFD modeling approaches that are widely used in describing flow in the human vasculature are discussed. A description will be provided of the computational pipeline. Finally, examples of applications to patient-specific conditions will be presented.

D. Saloner (✉)
Department of Radiology and Biomedical Imaging, University of California San Francisco, San Francisco, CA, USA
e-mail: David.Saloner@ucsf.edu

C. Yuan et al. (eds.), *Vessel Based Imaging Techniques*,
https://doi.org/10.1007/978-3-030-25249-6_17

Assessing the Velocity Field

In the same way that the motion of solid objects in space is described by Newton's equations of motion, fluid flow is described by the Navier-Stokes equations which include pressure terms and the fluid viscosity [1]. These equations can be used to describe fluid flow in a broad range of conditions including external flows (e.g., air flowing around the exterior of a vehicle) or internal flows (such as blood flowing in a blood vessel.) However, it is not possible to provide analytic solutions for the Navier-Stokes equations for any but a few limited geometries and conditions. For this reason, most practical approaches to describing details of hemodynamics rely on numerical simulations, referred to as Computational Fluid Dynamics (CFD). Initial CFD studies were developed in an era of limited computational power and used rudimentary numerical schemes. In the early applications of CFD to the study of vascular physiology, idealized representations of relevant anatomical structures were used [2]. Those began with 2D models which, while informative about important hemodynamic features, failed to capture important effects from secondary flow. The limitations of those models were recognized early on as the dominant role of geometry in governing critical features of hemodynamics became increasingly apparent. Extensions of the idealized models were developed to provide fully three-dimensional representations but were of limited use for patient-specific analyses [3, 4]. An example is presented in Fig. 17.1 of a schematic model of flow in the extracranial carotid arteries. The model is based on representative values of the bifurcation angle between the internal and external carotid arteries and uses typical values

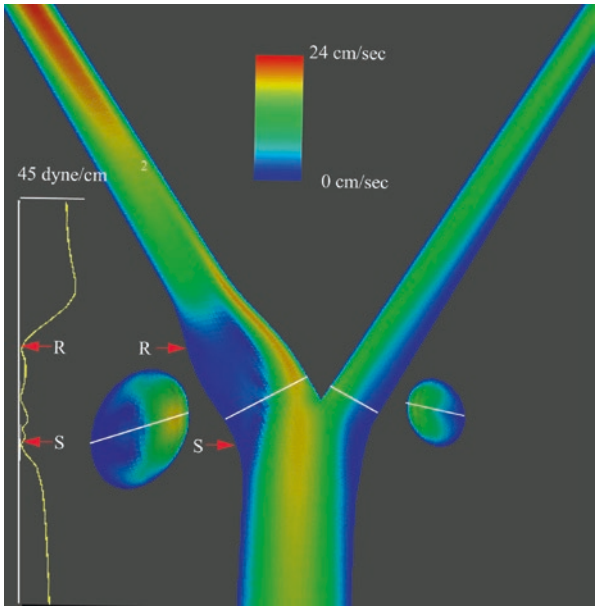

Fig. 17.1 A color-coded CFD-computed velocity field with high velocities encoded in red for a schematic representation of the extracranial carotid bifurcation. Slow recirculating flow in the bulb can be observed (blue region). A plot of the derived wall shear stress along the lateral wall of the internal carotid artery shows an extended area of low wall shear stress in the bulb from the point of flow separation (S) to reattachment (R)

for the diameters of each vessel. General features of the flow in that territory include slow recirculating flow in the bulb of the internal carotid artery and a high velocity region in the medial aspect of the internal carotid artery. Planes transverse to the proximal internal and external carotid arteries are also useful to show those features. Such idealized models became increasingly sophisticated with inclusion of compliant walls, features of wall disease, and modeling of varying blood viscosity properties [5, 6].

More recently, advances in computational methods have been included into commercial solvers with much of that development being spurred by applications to the aerospace, auto, and other industries where flow conditions are significantly more extreme than in the human vasculature. These solvers are now sufficiently sophisticated to readily incorporate realistic geometries and physiological flow conditions and can therefore be applied to patient-specific anatomy and flow.

Imaging Approaches

The interest in utilizing CFD methods in considerations of hemodynamics in vascular disease is manifold. While there are a variety of methods for assessing important features of hemodynamics in vivo, these have relatively coarse spatial and temporal resolution and suffer from technical and physiological challenges. Ultrasound is noninvasive and relatively inexpensive and has excellent temporal resolution for determining the full spectrum of velocities in a fixed insonation volume. It has strong abilities for quantifying peak velocities in flow jets which can be used to infer the degree of stenosis. It is unable to similarly map the velocity field through a three-dimensional volume and, in many cases, is obscured by bowel gas, calcifications, or overlying bone – as is the case for the brain. Furthermore, it is highly operator-dependent and is unsuited to measurement of volume flow. Catheter-injected angiography provides qualitative visualization of flow dynamics which is important for determining important physiological features such as vascular patency and the existence of collateral pathways. However, it is invasive and expensive and is not quantitative. MR imaging, particularly 4D Flow, has a number of desirable features: it is noninvasive and can depict the velocity field in space and time without limitations of overlying anatomy [7, 8]. This offers the possibility of determining derived descriptors such as volume flow and wall shear stress, the frictional force exerted by blood on the vessel wall. However, MR has moderate spatial and temporal resolution. Unlike ultrasound which determines the spectrum of velocities in the insonation volume, MR provides a voxel-averaged velocity measurement. Because of practical imaging constraints such as signal to noise ratios and acquisition times (which are often longer than 10 minutes), studies in a number of vascular territories are acquired with less than three or four voxels across the vascular lumen. The derivation of critical parameters such as the wall shear stress rely on an accurate measurement of the spatial gradient of velocities at the vessel wall, and MR-derived estimates of these measures must therefore be viewed with appropriate caution. A

major attraction of CFD methods is the ability to specify very high resolution in space and time and calculate velocity fields with resolution far beyond anything that is currently achievable with in vivo imaging methods.

Computational Fluid Dynamics (CFD)

In most vascular territories and under a broad range of healthy and pathologic states, a numerical solution of the Navier-Stokes equations can be attained with limited and reasonable assumptions. While methods exist to accommodate each of the following, they are often neglected in conventional CFD calculations of hemodynamics: the vessel wall is assumed to be rigid; blood is assumed to be a Newtonian fluid; and blood flow is considered to be laminar without the presentation of turbulence. With those assumptions, CFD calculations can be conducted if the surface boundary of the vascular structure of interest is specified, if the inlet flow waveform is defined, and if the outlet flow conditions are appropriately conditioned.

Vascular Compliance Returning to the major assumptions, the importance of neglecting vascular compliance is not fully understood given the difficulty in conducting a simulation that includes wall motion – a so-called fluid-structure interaction (FSI) problem [9]. Results of FSI compared to CFD with rigid walls indicate that neglecting compliance in a number of vascular territories (such as the intracranial vessels) has little effect [10]. In other territories such as the aorta, larger differences are reported [11]. It is, however, difficult to assess the extent to which the wall motion is correctly incorporated into the FSI models given their reliance on unreliable in vivo imaging to condition their boundary values. Furthermore, in conditions such as atherosclerosis, aneurysmal disease, or in the elderly population in general, resorting to an FSI simulation is likely unwarranted since vessels lose their compliance under those conditions, and conventional CFD methods are likely to suffice.

Newtonian Viscosity Fluid viscosity describes how the shear stress varies with changes in the shear rate, and if shear stress changes linearly with shear rate, the viscosity is constant. It is then referred to as a Newtonian fluid. Most CFD models assume that blood is a Newtonian fluid. There are in vivo situations where this condition is violated. On one limit, when blood recirculates slowly, red blood cells can aggregate, resulting in an increase in viscosity. Regions of slowly recirculating flow can occur in regions of aneurysmal dilatation. There are a number of analytical formulas that can be incorporated into CFD solvers that attempt to provide more physical models of blood viscosity at low shear rates [12]. There are reports that these effects are relatively small. On the other limit, the viscosity of blood decreases substantially when passing through narrow (<300 micron) vessels when red blood cells move to the center of the vessel leaving only plasma near the wall of the vessel (the Fåhraeus–Lindqvist effect). These vessels are of the scale of arterioles and capillaries and are generally not of current interest for the determination of detailed features in their velocity fields.

Turbulence The caliber and flow rates in healthy vessels are such that flow is laminar with the components of blood moving along well-ordered and predictable trajectories. Flow patterns can still be extremely complex with strong components of vorticity, but flow patterns remain highly predictable. As inertial effects, characterized by the product of velocity and vessel diameter, begin to dominate drag forces, characterized by viscosity, flow transitions from the well-ordered laminar condition to a more chaotic and unpredictable state and manifests as turbulent flow [13, 14]. Conditions that lend themselves to turbulent flow include flow distal to stenoses. Although velocities through the stenosis may increase dramatically, the reduced diameter can ensure that flow remains laminar in the stenosis throat. However, distal to the stenosis, high velocity persists in the flow jet which is now located in a region with a much larger diameter. Flow can then be turbulent with chaotic eddies being shed from the boundaries of the jet, generally accompanied by a dissipation of energy and an audible bruit [14]. Correct numerical simulation of this situation requires a far greater degree of complexity than is required for laminar flow. Models for including turbulence into CFD simulations range from imposition of some simplifying assumptions such as in the most widely used model of turbulence, the k-epsilon model, where it is assumed that the turbulence viscosity is isotropic. Although inclusion of turbulence models into CFD analysis of blood flow in vessels is computationally expensive, commercial codes generally provide a k-epsilon model option [1, 15, 16]. More accurate simulations can be rendered using large eddy simulations [16] or an approach referred to as direct numerical simulation (DNS) [14]. An example of the manifestation of turbulence in a DNS simulation is presented in Fig. 17.2 for flow through an idealized model of an arterial stenosis for flow through a regular cylindrical vessel with a slightly eccentric stenosis representing a 75% reduction in cross-sectional area. This presentation of velocity fluctuations shows a breakdown of the orderly flow in the flow jet into chaotic vortices several diameters distal to the throat of the stenosis. DNS simulations obtain their accuracy by directly computing all flow effects down to the smallest scales needed to accurately describe the relevant flow effects. They are thus extremely computationally intensive, and, while important in regimes such as hypersonic flow over airplane wings, DNS is rarely used in application to physiologic flows. In situations of high flow rates, such as distal to stenoses, flow conditions can be such that flow is no longer truly laminar, and the physics of flow dictates that flow becomes transitional and finally manifests true turbulence. In that case, it is challenging, and sometime

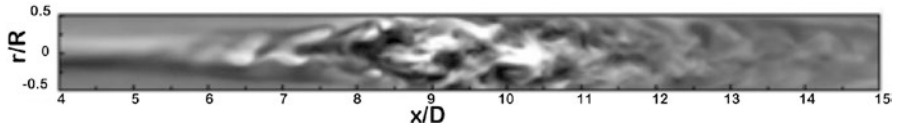

Fig. 17.2 A DNS simulation of flow in the longitudinal plane of a tube with a non-stenosed diameter D, and a 75% eccentric stenosis by area. Streamwise velocity fluctuations are shown (x) along the length of the vessel (x) between 4 and 15 diameters distal to the stenosis. This map shows the transition from regular to complex flow as the flow jet breaks into vortical eddies. (Varghese et al. [14], reproduced with permission)

impossible – even with an extremely high resolution – for code defined for laminar flow to converge to a stable solution, a situation that is manifested by increasingly long computational run times and inconsistent data. To avoid these types of computational failures, commercial CFD solvers are often constructed to include an artificial damping term which ensures that the solution remains stable. In that case, the user needs to realize that although a solution is generated, it is likely inaccurate, and appropriate caution must be used in drawing conclusions from those results.

In general, many physiological conditions of interest can be closely approximated by laminar flow through rigid-walled vessels with Newtonian viscosity. For those cases, conventional CFD simulations can then be applied to generate highly accurate estimates of the velocity field. However, in cases where those conditions are not met, in vivo imaging modalities, in particular 4D Flow MRI methods, provide the intriguing prospect of more accurately determining the velocity field than is possible with CFD as the true physiological behavior is inherently present on a patient-specific basis, and does not require modeling. In the remainder of this chapter, we will restrict ourselves to a discussion of the application of conventional CFD to the analysis of hemodynamics in vivo.

CFD in the Laminar Flow Regime

A CFD analysis provides a numerical solution of the Navier-Stokes equations, the governing equations of fluid motion. The key components required as input to the numerical model are a description of the lumenal surface of the vessels of interest and specification of the inlet and outlet flow boundary conditions.

Lumen Surface Patient-specific modeling requires in vivo images of the vessels of interest [17–19]. The resolution of the images must be sufficient to permit an accurate representation of the associated velocity fields – preferably with greater than five to ten voxels across the vascular lumen. Achieving this is most challenging in regions of pronounced curvature such as at the neck of a saccular aneurysm or in stenotic vessels. For example, an 80% diameter stenosis of the extracranial carotid arteries corresponds to a residual lumenal diameter of little more than 1 mm. For 3D volumetric modalities (MRA or CTA), this provides at most 2–3 voxels across the stenosis. This is even more limiting in territories with stenoses of smaller caliber vessels such as the coronary arteries or the intracranial vessels. However, current imaging modalities provide 3D angiographic images of the vascular lumen with high contrast to noise ratio to the adjacent tissue and with adequate spatial resolution to support high-quality CFD in relatively smooth vessels whose caliber is 3 mm or larger. Segmentation of the lumenal surface from the 3D data set can then be performed and be provided as input into the solver for the geometric boundary condition. Care is needed to avoid misrepresentations of important vascular features as in cases where aneurysmal bulges fold back into close proximity with the parent vessel. Unless the imaging modality has sufficient resolution, the two distinct

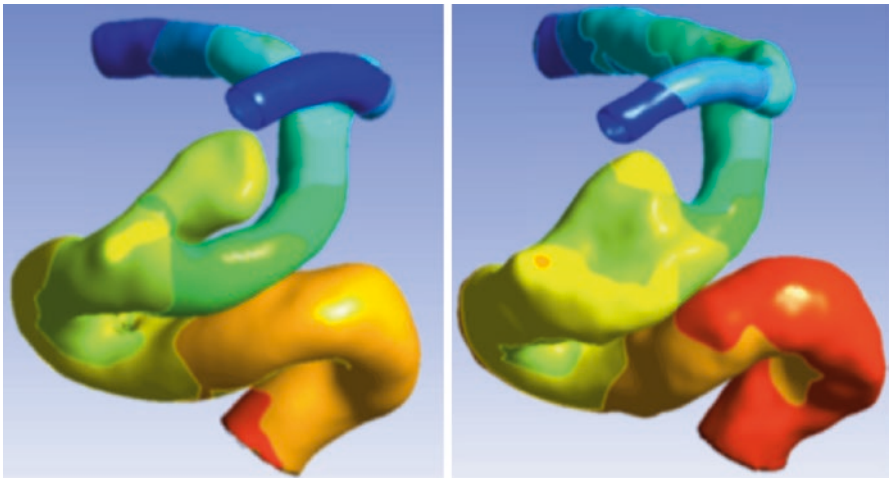

Fig. 17.3 Impact of acquisition resolution. CFD-calculated pressure distribution in a distal internal carotid artery with a cavernous segment aneurysm. Left: pressure map using surface segmentation from a rotational DSA study with 0.2 mm isotropic resolution clearly shows the separation between distal ICA and the aneurysm. Right: pressure map using surface segmentation from a CE-MRA study with 0.7 mm isotropic resolution fails to correctly resolve the inferior aspect of the aneurysm

regions can appear to be merged into one volume. This is illustrated in Fig. 17.3 where a rotational DSA study of an aneurysm of the internal carotid artery clearly identifies the aneurysm as a distinct saccular structure, whereas the lower resolution CE-MRA study merges aneurysm and parent vessel giving the appearance of a fusiform dilatation.

Flow Boundary Conditions In addition to specification of the surface geometry, it is important to provide suitable boundary conditions to define the inlet and outlet flow conditions. The inlet boundary condition is invariably provided by specifying the time-varying volume flow into the vessel of interest – optimally as measured in vivo at the corresponding location for the specific patient. If those are not available, idealized waveforms using representative volume flow values from the literature are often used. In order to have a realistic spatial distribution of velocities across the lumen, the inlet vessel can be extended proximal to the patient-specific domain a sufficient length to ensure that flow is fully developed. More complex models of inlet flow conditions have been formulated to account for cardiac dynamics [20]. Specification of the outlet boundary conditions depends on whether flow is monophasic or triphasic indicating the presence of a reflected wave as in the infrarenal aorta. For monophasic flow, it is sufficient to describe the outlet boundary condition by specifying zero pressure at the outlet. For locations where there is retrograde flow, more complicated modeling of the outlet conditions is required. The presence of retrograde flow indicates the presence of a compliant reservoir in the peripheral vessels or the distal vascular bed that is the source of the pressure that

drives the retrograde flow. Among the approaches used to model the outline boundary conditions has been the use of an electrical circuit analog of the downstream vasculature that consists of a resistance (R1) connected in series with a parallel combination of a second resistance,(R2), and a capacitance, (C) [21–24]. Care is required to appropriately model the values of the resistances and capacitance to ensure that the appropriate triphasic outlet waveform is reproduced [25]. Evaluations have been performed to investigate the sensitivity of computed flow fields to different models of the outlet flow conditions [26]. Models have also been developed that compare flow conditions under different physiology, such as different exercise regimens [24].

CFD Computational Framework

The computation of the velocity field for a patient-specific representation begins with a segmentation of the vascular surface from in vivo imaging. The marching cubes algorithm can be used to render the segmented surface of the lumen as a polygonal (triangular) mesh [27]. In CFD the Navier-Stokes equations are solved at a number of discrete points within a defined computational domain, and it is therefore necessary to create a mesh whereby the fluid volume is discretized into cells [28]. A variety of different techniques have been formulated to perform these simulations with both finite difference and finite volume methods having enjoyed wide use [29]. In both cases, the computational domain is resolved into a network of nodes and elements. The finite element method utilizes approximations of derivatives using the Taylor expansion and requires a structured mesh that is uniform and highly regular. It is therefore inflexible and difficult to implement for realistically complex geometries and the finite volume, which is more flexible is more commonly used. The finite volume method converts the governing equations into algebraic equations that can be numerically solved over discrete control volumes throughout the computational domain. Average values for each cell are calculated by computing fluxes through the cell faces. Conservation of physical properties is ensured as the computational algorithms enforce that flux into the cell element equals the flux out of the cell. With this approach it is no longer necessary to solve on a uniform structured mesh. Semiautomated tools for generating unstructured meshes now exist that can create the computational nodes needed with a specified mesh density [30]. The use of increasingly finer meshes ensures not only better resolution of the structure of the flow fields but inherently more accurate [31]. However, computational times can become prohibitively lengthy if the mesh density is excessive. On the other hand, if the mesh density is insufficient, computational errors can result. In order to have high confidence in the CFD results, it is important to incrementally refine the mesh density to ensure that the calculated velocity fields converge to an acceptable residual error [32]. Careful construction of the mesh can serve to provide a compromise between high accuracy and speed of computation by prescribing variable mesh density. High-density mesh elements can be prescribed

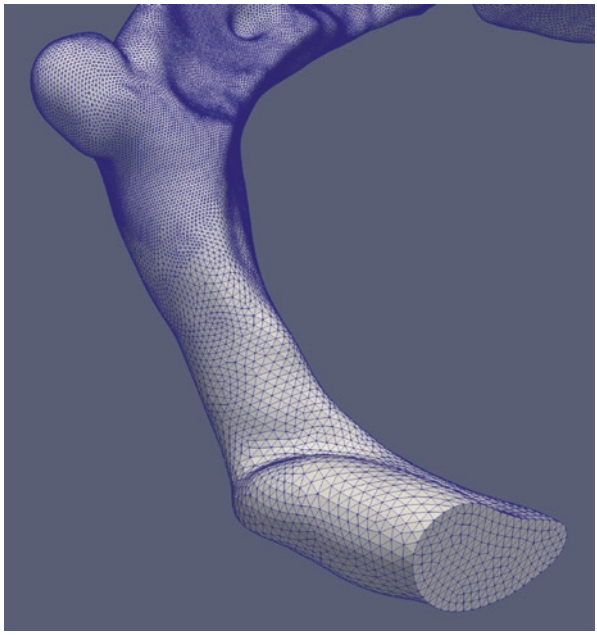

Fig. 17.4 Mesh generated through the volume defined by the surface segmented from an MRA study of the transverse and sigmoid sinus of a subject with venous diverticulum. A spatially varying mesh is defined with high mesh density proximal to and through the diverticulum and with low mesh density in the more uniform segment of anatomy

where these are most needed, such as at locations of high surface curvature or irregularity or close to the vessel wall where gradients of velocity must be determined to provide rigorous estimates of wall shear stress [33]. On the other hand, velocities in the center of low-curvature segments of a vessel are expected to vary smoothly, and low mesh densities can be used there. An example showing a spatially adaptive mesh designed to provide increased accuracy in regions requiring higher sensitivity is shown in Fig. 17.4.

Application to Vascular Disease

The great promise of methods that provide quantitative hemodynamic measures lies in the potential of those methods to serve as biomarkers for the increased likelihood of disease progression [34]. If, indeed, hemodynamic forces are drivers of disease evolution over time, it is reasonable to assume that a careful analysis of hemodynamic descriptors could serve to identify, on a patient-specific basis, individuals who are likely to show rapid disease progression and others where the condition is expected to remain stable over time. Extensive work is being actively pursued to establish the relationship between hemodynamic descriptors and disease progression. Those studies can be quite challenging in cases where the disease condition does not have high prevalence, where the disease evolution is slow and potentially occurring over decades, and where rigorous clinical outcomes – such as aneurysm rupture – need to be established. This analysis is further complicated by

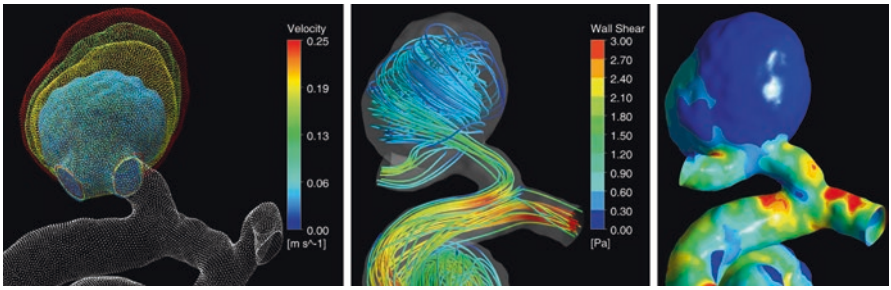

Fig. 17.5 CFD in a growing aneurysm of the anterior communicating artery. Left: four serial MRA studies show interval growth from baseline (blue) to 18-month follow-up scan (red). Center: flow streamlines generated from CFD-computed velocity field shows strong recirculating flow in the aneurysm. Right: wall shear stress map from CFD-computed velocity field shows low wall shear stress (deep blue) colocalizing with region of observed growth

the wide variety of secondary descriptors that can be, and have been, postulated to be the critical markers. These descriptors include intravascular pressure; zones of jet impingement; wall shear stress (which can be further investigated in terms of peak wss, mean wss, or OSI – the oscillating shear index which characterizes the variation of wss through the cardiac cycle); presentation and number of vortices; and the extent of the deposition of turbulent kinetic energy – to name a few [18, 35–39]. Insights into the roles of the different descriptors do not necessarily need to be based solely on clinical outcomes (such as stroke or myocardial infarction) but can be gleaned from longitudinal imaging studies where evolution of vascular geometry can be detected [19]. Figure 17.5 presents results from a study where a patient with an untreated aneurysm of the anterior communicating artery was followed with noninvasive CE-MRA at 6-month intervals for a total of four imaging sessions. The sequential studies are spatially colocalized and visualized with a transparent mesh showing a near doubling on volume of the aneurysm over an 18-month period. Also shown are the CFD-computed flow streamlines (presented for the final imaging timepoint) and the derived wall shear stress map. In this case, the region of pronounced growth is seen to colocalize with the region of low wall shear stress.

As noted above, an alternative to CFD is to directly measure the velocity field using 4D MR Flow. While that approach circumvents the need to develop the entire computational pipeline, it faces the inaccuracies of the acquisition, specifically the limited spatial and temporal resolution. These differences can be noted when comparing visual representation of streamlines from CFD with those from 4D Flow for the same geometry. Streamlines are a common method of displaying qualitative visualizations of the prevailing flow and are created at fixed points of time in the cardiac cycle by tracing out the path followed through the domain as dictated by the velocity field. To the extent that there is limited resolution of inconsistencies in the predicted velocity field, streamlines will follow irregular paths and will have variable filling of the flow domain. Figure 17.6 shows streamlines generated from a CFD simulation based on a CE-MRA acquired from a patient

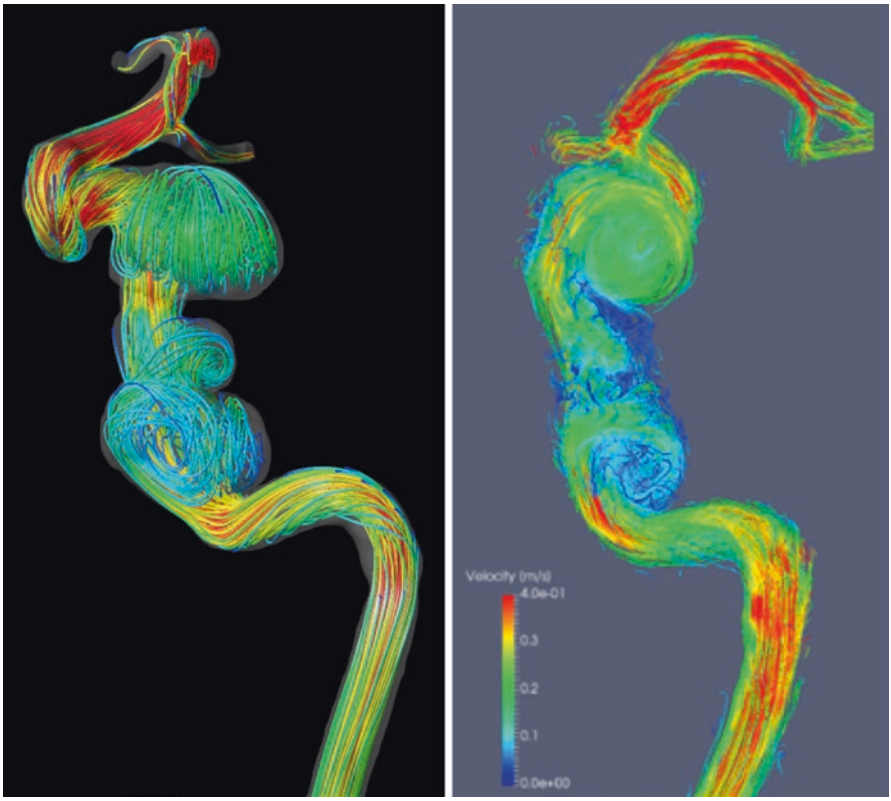

Fig. 17.6 Study of a patient with three aneurysms of the internal carotid artery comparing streamlines from CFD simulations with those from 4D Flow demonstrating that CFD is noise-free. Left: streamlines generated from the CFD-calculated velocity map based on the boundary conditions from the in vivo CE-MRA and the flow waveform measured with 2D PC-MRI in the proximal ICA. Right: streamlines generated from a 4D Flow PC-MRI study

with three aneurysms of the internal carotid artery and from a 4D Flow study on the same patient. The CFD-based streamlines are smooth and uniform, whereas the 4D Flow-based streamlines are noisy.

There is a great deal of interest in using CFD to investigate the effects of planned interventions [40]. To the extent that the intervention makes significant changes to flow conditions, this is clearly a situation where pre-treatment imaging plays little role. On the other hand, CFD can be used to estimate what the probable results of surgical interventions might be [41, 42]. The validity of such predictions, however, depends importantly on the boundary conditions that will exist following surgery. In certain cases, reasonable assumptions can be made based on considerations of normal physiology, as for example in a planned bypass procedure where it is expected that the intervention will restore normal flow to the distal organ. Other considerations include using vessel caliber of the targeted bypass implantation site as a predictor of what the likely flow into that vessel will be. In other

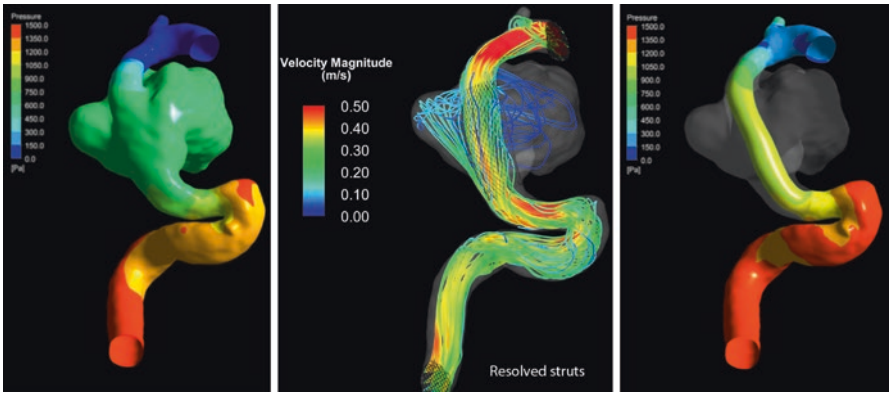

Fig. 17.7 CFD calculation of a simulation that models deployment of a flow diverter stent in a distal ICA aneurysm. Left: CFD-calculated pressure map in the untreated aneurysm. Center: streamlines calculated with modeling of the deployed flow diverter. Right: CFD-calculated pressure map for the simulated treatment

scenarios, predictive simulations are better able to incorporate the actual geometric and functional morphology that will result from intervention. Examples are simulations that have been performed to evaluate the impact of deploying different numbers of coils to treat an aneurysm [43], or others that estimate the likelihood that a flow-diverting stent deployed through a fusiform aneurysm will reduce flow into the aneurysm sac thereby promoting thrombotic occlusion of the sac [44–47]. In that case, the flow boundary conditions following treatment can be clearly defined, and the geometry of elements of the deployed stent – which is well known – can be included in the simulation. Figure 17.7 shows modeling of planned treatment in a fusiform aneurysm. Not only is CFD able to predict the pressure distribution in the presenting anatomy prior to intervention, but careful inclusion of the detailed geometry of the deployed flow-diverting stent permits prediction of the flow streamlines and pressure map in the vasculature following stent deployment. This example shows a strong reduction of flow into the aneurysmal sac through the pipeline walls.

An additional strength of CFD is to explore flow conditions across a range of conditions that are not amenable to variation in vivo [48, 49]. Vortical flow has been postulated as a contributor to audible sound in patients with pulsatile tinnitus. In vivo assessment of flow is able to establish the presence of a strong component of vorticity inflow in the bulb of the jugular vein. However, the extent to which the relationship between the geometric structure of the bulb and the total volume flow through the vein plays a role in determining the presence of flow vorticity is unknown. CFD can be performed for the given geometry but with incremental reduction of the inlet flow conditions from what presents in vivo until a flow rate where the vorticity is no longer detected. This is illustrated in

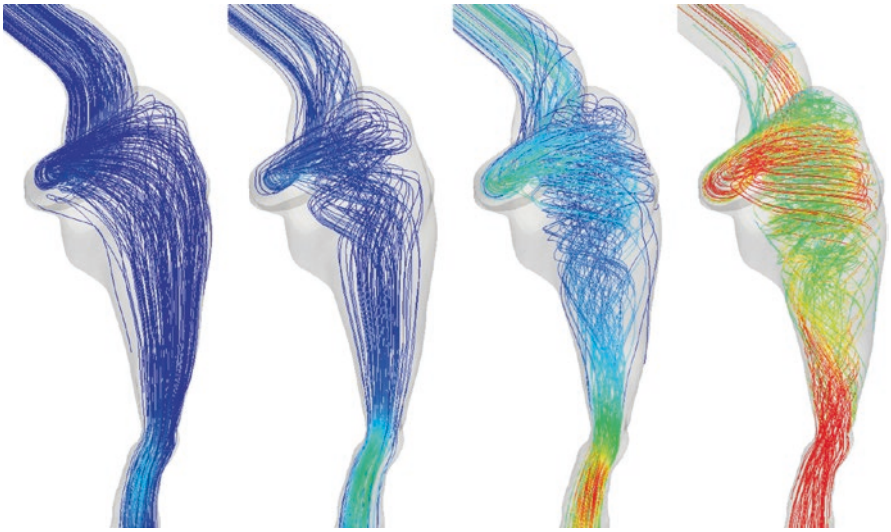

Fig. 17.8 Flow streamlines generated from CFD for flow through a patient-specific model of the jugular vein. This demonstrates the ability to explore flow conditions in simulation that do not present in vivo. Streamlines are displayed with incremental adjustment of the inlet flow from a slow flow rate on the left to the flow rate measured in vivo, on the right. A strong rotational component of flow is visualized in the jugular vein at all conditions apart from the slowest (and highly non-physiologic) flow rate on the left

Fig. 17.8. Flow streamlines were calculated for the geometry and inlet waveform, as detected from CE-MRA and 2D phase-contrast MRI, respectively, in the jugular vein of a patient with pulsatile tinnitus. In addition, the volume flow was reduced in simulation until the vortical flow disappeared showing, in this case, that the vorticity was largely dominated by the flow geometry and was only absent at very low flow rates.

The high fidelity of CFD data permits the use of advanced algorithms for extracting features of flow that are not immediately available from the calculated velocity field [50]. An additional metric that is of interest in vascular disease is the potential for flow conditions to result in intraluminal thrombus deposition [44]. A convenient metric for that is the particle residence time. Particle residence time bears some similarities to the passage of contrast material injected intra-arterially during dynamic catheter angiography runs, particularly in the late phase as the contrast washes out. It is possible to utilize the data generated by the CFD-calculated velocity field to create a visualization of what the expected wash out of material in the modeled geometry will be, and hence, in effect, display the particle residence time. Figure 17.9 is a series of estimated contrast distributions in a fusiform aneurysm of the vertebral-basilar system following complete opacification of the territory. Serial time windows show the contrast as it is transported out of the vessel.

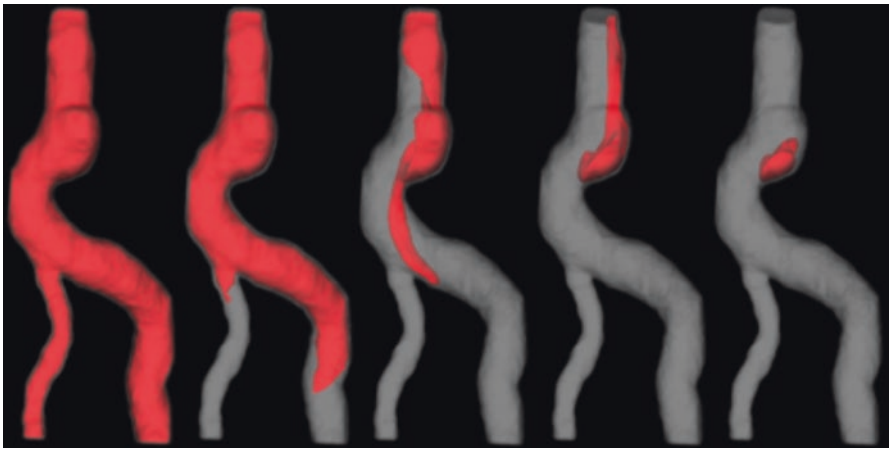

Fig. 17.9 Contrast passage through an aneurysmal segment distal to the vertebral-basilar junction. A virtual injection of contrast material is shown in red within the lumenal geometry (gray). These images estimate from the CFD-computed velocity field, the washout of contrast from full opacification (left) to late in the injection run (right) showing extended dwell time of contrast in the aneurysmal dilation

Conclusion

Computational Fluid Dynamics is a powerful methodology for providing highly accurate estimates of the hemodynamics on a patient-specific basis. This approach will remain the gold standard for defining velocity fields until in vivo imaging modalities attain greater resolution than they currently provide. CFD can be used to generate biomarkers that can be used to assess the risk posed by vascular dysfunction on a patient-specific basis. Commercial codes are available that are suitable for application to in vivo physiology. Current CFD models make important assumptions, and care should be taken when relying on CFD-generated data to evaluate the extent to which the actual in vivo conditions are consistent with the underlying assumptions. Finally, CFD presents the potential to model the hemodynamic outcomes of planned vascular revisions, providing the treating surgeon with quantitative data on which to base their treatment.

References

1. Ferziger J, Peric M. Computational methods for fluid dynamics. Berlin: Springer-Verlag; 1996.
2. Jou L, Berger S. Numerical simulation of the flow in the carotid bifurcation. Theor Comput Fluid Dyn. 1998;10:239–48.
3. Perktold K, Resch M, Florian H. Pulsatile non-Newtonian flow characteristics in a three-dimensional human carotid bifurcation model. J Biomech Eng. 1991;113(4):464–75.

4. Perktold K, Resch M, Peter RO. Three-dimensional numerical analysis of pulsatile flow and wall shear stress in the carotid artery bifurcation. J Biomech. 1991;24(6):409–20.
5. Perktold K, Thurner E, Kenner T. Flow and stress characteristics in rigid walled and compliant carotid artery bifurcation models. Med Biol Eng Comput. 1994;32(1):19–26.
6. Stroud JS, Berger SA, Saloner D. Numerical analysis of flow through a severely stenotic carotid artery bifurcation. J Biomech Eng. 2002;124(1):9–20.
7. Dyverfeldt P, Bissell M, Barker AJ, Bolger AF, Carlhall CJ, Ebbers T, et al. 4D flow cardiovascular magnetic resonance consensus statement. J Cardiovasc Magn Reson. 2015;17:72.
8. Garcia J, van der Palen RLF, Bollache E, Jarvis K, Rose MJ, Barker AJ, et al. Distribution of blood flow velocity in the normal aorta: effect of age and gender. J Magn Reson Imaging. 2018;47(2):487–98.
9. Cebral JR, Yim PJ, Lohner R, Soto O, Choyke PL. Blood flow modeling in carotid arteries with computational fluid dynamics and MR imaging. Acad Radiol. 2002;9(11):1286–99.
10. Dempere-Marco L, Oubel E, Castro M, Putman C, Frangi A, Cebral J. CFD analysis incorporating the influence of wall motion: application to intracranial aneurysms. Med Image Comput Comput Assist Interv. 2006;9(Pt 2):438–45.
11. Lantz J, Renner J, Karlsson M. Wall shear stress in a subject specific human aorta — influence of fluid-structure interaction. J Appl Mech. 2011;3:759–78.
12. Gijsen FJ, van de Vosse FN, Janssen JD. The influence of the non-Newtonian properties of blood on the flow in large arteries: steady flow in a carotid bifurcation model. J Biomech. 1999;32(6):601–8.
13. Chien KY. Predictions of channel and boundary-layer flows with a low-Reynolds-number turbulence model. AIAA J. 1982;20(1):33–8.
14. Varghese SS, Frankel SH, Fischer PF. Direct numerical simulation of stenotic flows. Part I steady flow. J Fluid Mech. 2007;582:253–80.
15. Ferziger J. Large eddy numerical simulations of turbulent flows. AIAA J. 1977;15(9):1261–7.
16. Ghosal S, Lund T, Moin P, Selvoll K. A dynamic localization model for large-eddy simulation of turbulent flows. J Fluid Mech. 1995;286:229.
17. Long Q, Xu XY, Bourne M, Griffith TM. Numerical study of blood flow in an anatomically realistic aorto-iliac bifurcation generated from MRI data. Magn Reson Med. 2000;43(4):565–76.
18. Cebral JR, Duan X, Chung BJ, Putman C, Aziz K, Robertson AM. Wall mechanical properties and hemodynamics of unruptured intracranial aneurysms. AJNR Am J Neuroradiol. 2015;36(9):1695–703.
19. Boussel L, Rayz V, McCulloch C, Martin A, Acevedo-Bolton G, Lawton M, et al. Aneurysm growth occurs at region of low wall shear stress: patient-specific correlation of hemodynamics and growth in a longitudinal study. Stroke. 2008;39(11):2997–3002.
20. Kim HJ, Vignon-Clementel IE, Figueroa CA, LaDisa JF, Jansen KE, Feinstein JA, et al. On coupling a lumped parameter heart model and a three-dimensional finite element aorta model. Ann Biomed Eng. 2009;37(11):2153–69.
21. Kung EO, Les AS, Medina F, Wicker R, McConnell MV, Taylor CA. In vitro validation of finite-element model of AAA hemodynamics incorporating realistic outlet boundary conditions. J Biomech Eng. 2011;133:1003–11.
22. Kung EO, Taylor CA. Development of a physical windkessel module to re-create in-vivo vascular flow impedance for in-vitro experiments. Cardiovasc Eng Technol. 2011;2(1):2–14.
23. Taylor CA, Figueroa CA. Patient-specific modeling of cardiovascular mechanics. Annu Rev Biomed Eng. 2009;11:109–34.
24. Les AS, Shadden SC, Figueroa CA, Park JM, Tedesco MM, Herfkens RJ, et al. Quantification of hemodynamics in abdominal aortic aneurysms during rest and exercise using magnetic resonance imaging and computational fluid dynamics. Ann Biomed Eng. 2010;38(4):1288–313.
25. Romarowski RM, Lefieux A, Morganti S, Veneziani A, Auricchio F. Patient-specific CFD modelling in the thoracic aorta with PC-MRI-based boundary conditions: a least-square three-element Windkessel approach. Int J Numer Method Biomed Eng. 2018;34(11):e3134.

26. Pirola S, Cheng Z, Jarral OA, O'Regan DP, Pepper JR, Athanasiou T, et al. On the choice of outlet boundary conditions for patient-specific analysis of aortic flow using computational fluid dynamics. J Biomech. 2017;60:15–21.
27. Lorensen W, Cline HE. Marching cubes: a high resolution 3D surface construction algorithm. ACM SIGGRAPH Comput Graph. 1987;21:163.
28. Cebral JR, Lohner R, Choyke PL, Yim PJ. Merging of intersecting triangulations for finite element modeling. J Biomech. 2001;34(6):815–9.
29. Jeong W, Seong J. Comparison of effects on technical variances of computational fluid dynamics (CFD) software based on finite element and finite volume methods. Int J Mech Sci. 2014;78:19–26.
30. Berg P, Janiga G, Thévenin D. Detailed comparison of numerical flow predictions in cerebral aneurysms using different CFD software 2012.
31. Zhou Y, Lee C, Wang J. The computational fluid dynamics analyses on hemodynamic characteristics in stenosed arterial models. J Healthc Eng. 2018;2018:4312415.
32. Khan MO, Valen-Sendstad K, Steinman DA. Narrowing the expertise gap for predicting intracranial aneurysm hemodynamics: impact of solver numerics versus mesh and time-step resolution. AJNR Am J Neuroradiol. 2015;36(7):1310–6.
33. Valen-Sendstad K, Piccinelli M, Steinman DA. High-resolution computational fluid dynamics detects flow instabilities in the carotid siphon: implications for aneurysm initiation and rupture? J Biomech. 2014;47(12):3210–6.
34. Liang L, Steinman DA, Brina O, Chnafa C, Cancelliere NM, Pereira VM. Towards the clinical utility of CFD for assessment of intracranial aneurysm rupture - a systematic review and novel parameter-ranking tool. J Neurointerv Surg. 2019;11(2):153–8.
35. Botnar R, Rappitsch G, Scheidegger MB, Liepsch D, Perktold K, Boesiger P. Hemodynamics in the carotid artery bifurcation: a comparison between numerical simulations and in vitro MRI measurements. J Biomech. 2000;33(2):137–44.
36. Burleson A, Strother C, Turitto V. Computer modeling of intracranial saccular and lateral aneurysms for the study of their hemodynamics. Neurosurgery. 1995;37(4):774–84.
37. Burleson AC, Turitto VT. Identification of quantifiable hemodynamic factors in the assessment of cerebral aneurysm behavior. On behalf of the Subcommittee on Biorheology of the Scientific and Standardization Committee of the ISTH. Thromb Haemost. 1996;76(1):118–23.
38. Cebral JR, Mut F, Weir J, Putman CM. Association of hemodynamic characteristics and cerebral aneurysm rupture. AJNR Am J Neuroradiol. 2011;32(2):264–70.
39. Jou LD, Mawad ME. Timing and size of flow impingement in a giant intracranial aneurysm at the internal carotid artery. Med Biol Eng Comput. 2011;49(8):891–9.
40. Cebral JR, Mut F, Raschi M, Scrivano E, Ceratto R, Lylyk P, et al. Aneurysm rupture following treatment with flow-diverting stents: computational hemodynamics analysis of treatment. AJNR Am J Neuroradiol. 2011;32(1):27–33.
41. Acevedo-Bolton G, Jou LD, Dispensa BP, Lawton MT, Higashida RT, Martin AJ, et al. Estimating the hemodynamic impact of interventional treatments of aneurysms: numerical simulation with experimental validation: technical case report. Neurosurgery. 2006;59(2):E429–30; author reply E-30.
42. Aneis M, Stancampiana AP, Wakhloo AJ, Lieber BB. Modeling of flow in a straight stented and non-stented side wall aneurysm model. J Biomech Eng. 1997;119:206–12.
43. Groden C, Laudan J, Gatchell S, Zeumer H. Three-dimensional pulsatile flow simulation before and after endovascular embolization of a terminal cerebral aneurysm. J Cereb Blood Flow Metab. 2001;21:1464–71.
44. Bluestein D, Niu L, Schoephoerster RT, Dewanjee MK. Steady flow in an aneurysm model: correlation between fluid dynamics and blood platelet deposition. J Biomech Eng. 1996;118:280–6.
45. Hirabayashi M, Ohta M, Rufenacht DA, Chopard B. Lattice Boltzmann analysis of the flow reduction mechanism in stented cerebral aneurysms for the endovascular treatment. Lect Notes Comput Sci. 2003;2657:1044–53.

46. Hirabayashi M, Ohta M, Rufenacht DA, Chopard B. Characterization of flow reduction properties in an aneurysm due to a stent. Phys Rev E Stat Nonlinear Soft Matter Phys. 2003;68(2):1918.
47. Hodis S, Ding YH, Dai D, Lingineni R, Mut F, Cebral J, et al. Relationship between aneurysm occlusion and flow diverting device oversizing in a rabbit model. J Neurointerv Surg. 2016;8(1):94–8.
48. Taylor CA, Draney J, Ku DN, Parker D, Steele BN, Wang K, et al. Predictive medicine: computational techniques in therapeutic decision-making. Comput Aided Surg. 1999;4:231–47.
49. Jou LD, Quick CM, Young WL, Lawton MT, Higashida R, Martin A, et al. Computational approach to quantifying hemodynamic forces in giant cerebral aneurysms. AJNR Am J Neuroradiol. 2003;24(9):1804–10.
50. Cebral JR, Mut F, Chung BJ, Spelle L, Moret J, van Nijnatten F, et al. Understanding angiography-based aneurysm flow fields through comparison with computational fluid dynamics. AJNR Am J Neuroradiol. 2017;38(6):1180–6.